Atmospheric Environment 243 (2020) 117868

Contents lists available at ScienceDirect

Atmospheric Environment

journal homepage: http://www.elsevier.com/locate/atmosenv

Developing a statistical model to explain the observed decline of atmospheric mercury

Qingru Wu [a,b,1], Yi Tang [a,1], Shuxiao Wang [a,b,*], Liang Li [c], Ke Deng [d], Guigang Tang [c], Kaiyun Liu [a], Dian Ding [a], Hui Zhang [e]

[a] School of Environment, State Key Joint Laboratory of Environmental Simulation and Pollution Control, Tsinghua University, Beijing, 100084, China
[b] State Environmental Protection Key Laboratory of Sources and Control of Air Pollution Complex, Beijing, 100084, China
[c] China National Environmental Monitoring Center, No. 8 Anwai Dayangfang, Beijing, 100012, China
[d] Center for Statistical Science, Tsinghua University, Beijing, 100084, China
[e] State Key Laboratory of Environmental Geochemistry, Institute of Geochemistry, Chinese Academy of Science, 99 Lincheng West Road, Guiyang, 550081, China

HIGHLIGHTS

- TGM concentrations in Beijing decreased at a rate of −8% yr^{-1} from 2015 to 2018.
- GAM was developed to explain the decline of TGM concentrations in Beijing.
- Reduction of anthropogenic emission explained 51.5% of the decrease of TGM.

GRAPHICAL ABSTRACT

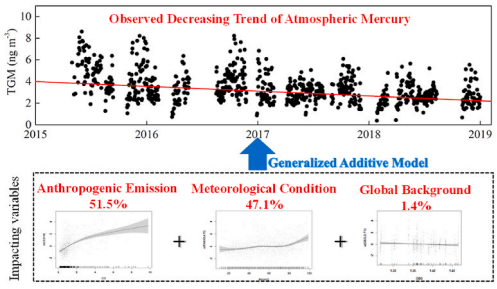

ARTICLE INFO

Keywords:
Atmospheric mercury concentration
Sen's slope
Generalized additive model
Mercury emissions
Meteorological condition

ABSTRACT

Mercury is a ubiquitous environmental toxicant and a cause for global concern due to its persistence and bioaccumulation in the environment. Evaluating the effectiveness of mercury emission control has become a significant issue after the entry into force of the *Minamata Convention on Mercury* in 2017. Atmospheric mercury concentration is an important indicator for anthropogenic emission control. Although Eulerian models are generally applied to evaluate emission reduction and policy effectiveness, the uncertainty of mercury reaction mechanisms and the insufficient grid accuracy of simulations limit the applications of this method at particular sites. In this study, we applied a statistical approach (the Generalized Additive Model, GAM) to explain the decline of atmospheric mercury concentration in Beijing, China, which followed a trend (Sen's slope) of −0.37 ng m^{-3} yr^{-1} (−8.0% yr^{-1}). The statistical model represented 56.5% of the variance in mercury concentration and the adjusted R^2 reached 0.547. Reduction of anthropogenic mercury emission, variation in meteorological condition, and change in global background level explained 51.5%, 47.1%, and 1.4% of the decrease of air mercury concentration, respectively. We validated the results using Hg emission inventories, seasonal Hg/CO value, and meteorological data. Considering the limitations of Eulerian models and the simplicity of statistical

* Corresponding author. School of Environment, State Key Joint Laboratory of Environmental Simulation and Pollution Control, Tsinghua University, Beijing, 100084, China.
E-mail address: shxwang@tsinghua.edu.cn (S. Wang).
[1] These authors have equal contribution.

https://doi.org/10.1016/j.atmosenv.2020.117868
Received 22 March 2020; Received in revised form 9 August 2020; Accepted 17 August 2020
Available online 22 August 2020

models, we suggest the application of GAM as an assessment method for long-term variation of atmospheric mercury.

1. Introduction

Mercury (Hg) is of great concern due to its biotoxicity and neurotoxicity, as Hg emissions can cause global pollution through long-range transport by air. To protect human health and the environment, global actions have been taken to reduce atmospheric Hg emissions (UNEP, 2013). With the 2017 entry into force of the *Minamata Convention on Mercury*, regional emissions are expected to be better controlled (Liu et al., 2019; Pacyna et al., 2016; Wu et al., 2016, 2018a, 2018b; Zhang et al., 2016). Methods for evaluating the effectiveness of Hg emission control became an important issue after the implementation of the convention.

Atmospheric Hg concentration is a significant indicator for evaluating the effectiveness of Hg emission control (Cole et al., 2013; Fu et al., 2015; Tang et al., 2018; Tong et al., 2016; Weigelt et al., 2015; Zhang et al., 2016). However, changes in atmospheric Hg concentrations are affected not only by anthropogenic activities, but also by meteorological conditions and global background concentrations (GBC). In order to quantitatively characterize the impact of anthropogenic Hg emissions on changes in ambient atmospheric Hg concentrations, previous studies have often used atmospheric Hg transport models based on Eulerian models, such as GLEMOS, ECHMERIT, GEMMACH-Hg, GEOS-Chem, and CMAQ-Hg (Pacyna et al., 2016; Selin et al., 2008; Ye et al., 2018). These models use atmospheric Hg inventories as the primary input data, then consider the impact of meteorological fields as well as physical and chemical mechanisms (Selin et al., 2008). By designing scenarios, the contribution of the selected parameters to changes in atmospheric Hg concentration can be quantitatively characterized. These models have performed well at both global and regional scales (Horowitz et al., 2017; Liu et al., 2019; Saiz-Lopez et al., 2018; Zhang et al., 2016). However, when they are applied to explain atmospheric Hg observations from a single site, their utility is often limited in two ways. First, uncertainty in the model mechanism itself leads to insufficient interpretation of observational data by the simulation results. Second, the dilution effect of gridding on atmospheric Hg concentration often makes the simulation results at urban stations significantly lower than the observed concentrations (Liu et al., 2019).

Statistical regression models are otherwise more flexible than Eulerian models. From a statistical perspective, the interpretation of factors affecting variations in target air pollutant is an issue with regression analysis, which is a set of statistical processes used for estimating the relationship between a dependent variable and one or more independent variables (Wood, 2017). There are different ways to model the conditional expectation function, including parametric, nonparametric, and semi-parametric approaches. Parametric approaches such as linear functions are an easy statistical method, but it is not clear that the relationship is linear in many cases (Li et al., 2019; Tai et al., 2010). Nonparametric regression is a much more robust approach, but it requires more calculations and a large number of samples; further, the model cannot be easily stabilized due to its high complexity. As a compromise between these two models, the semi-parametric approach is widely used in air pollution research. For example, the Generalized Additive Model (GAM) can be used to incorporate both linear and nonlinear parameters (Wood, 2017). GAM has been used to simulate long-term change trends of sulfur and nitrogen species, particulate matter (PM) concentrations (Aldrin and Haff, 2005; Holland et al., 2000), benzene and 1,3-butadiene concentrations (Reiss, 2006), and the maximum daily 8 h average ozone (Davis and Speckman, 1999; Gong et al., 2017). These analyses principally focused on exploring how concentrations were influenced by a wide range of meteorological and source-related variables.

Compared to the air pollutants mentioned above, the residence time of total gaseous Hg (TGM) is much longer and the global background also affects changes in atmospheric Hg concentrations at studied sites. In addition, the GAM parameters used in some studies include only meteorological factors and the residuals were identified as anthropogenic emissions (Aldrin and Haff, 2005; Li et al., 2019; Tai et al., 2010). When emissions are not the dominant source of target air pollutants, the GAM can accurately explain the target variables. However, when emissions change significantly, the lack of the first crucial independent variable reduces the proportion of variation of the dependent variable. In other words, this reduces the interpretation of existing independent variables to dependent variables and lowers the feasibility of the model. Therefore, when using the GAM to evaluate the effectiveness of atmospheric Hg reduction, it is also necessary to determine the independent variables that can be used to characterize emissions.

In this study, we applied GAM to explain variations in observed TGM concentration in Beijing, China by coupling the model with parameters representing GBC, anthropogenic emissions, and meteorological conditions. We used the Hg concentrations observed in Beijing as a case study and interpreted model results using the seasonal Hg/CO ratio, Hg emission inventories, meteorological data, and GBC. Our results demonstrate a rapid method for explaining site-specific observational data and can be used to assess the environmental benefits of Hg emission control on a city or regional scale.

2. Methodology

2.1. GAM model development

GAM produces a simple and explicit formulation of response-predictor relationships in a neural network framework (Aldrin and Haff, 2005). We simulated TGM in Beijing by using GAM in R software with the "mgcv" package (Wood, 2017). The GAM equation is as follows:

$$g(\mu i) = Xi\theta + f1(x1i) + f2(x2i) + \ldots + fn(xni) + \xi i, \quad (1)$$

where i is the observation on the ith day; g is the link function; and μ_i is the expectation of the dependent variable, which specifies the relationship between the linear formulation on the right side of the equation and the response μ_i. We used the "identity link" function with Gaussian distribution because the relationship between atmospheric Hg concentrations and parameters conformed to a Gaussian distribution and the estimation of GAM was considered unbiased (Figure S1). $X\theta$ is a constant component of the model, presenting a categorical relationship for predictors not subject to nonlinear transformation. $f(x)$ is the smooth function of the predictors. Penalized Cubic Regression Splines were used for the smoothing function to ensure a balance between underfitting the observed data and overfitting the data by choosing the effective number of degrees of freedom. The restricted maximum likelihood approach was used to estimate the smooth function.

The Akaike Information Criterion (AIC) was used as an estimator to ensure the effectiveness of each input variable. Higher R^2 and lower AIC values suggest better parameter selection and fitting results. We carried out backward selection coupling with the double penalty approach to ensure that all selected parameters were significant (by p value). Based on this method, we tested 15 variables and selected 9 final variables for the model (Table S1). These included one air pollutant variable (CO), GBC (reflecting the impact of global emissions), and seven meteorological variables. The latter included the backward trajectory longitude after 24 h ($Traj_{Long}$), daily average wind speed (V_{AVG}), daily average relative humidity (RH_{AVG}), daily temperature difference (T_{DELTA}), daily average surface pressure (P), daily average of temperature at 700 hPa

(T_{700}), and day of year (DOY). The latter represented the variation of TGM during a year and showed the influence of synthetical seasonal meteorological conditions. The significance of the independent variables was identified using F statistics (Table S2). The partial response curve of the independent variables was used to explain their nonlinear/linear relationship with TGM.

2.2. Variables and data sources

TGM data were measured from the roof of the China Environmental Monitoring Station, Beijing (40.04° N, 116.41° E), between May 2015 and December 2018 (Figure S2). This site, which lies on the northern side of the city without any industrial point sources within a 30 km radius, is a national atmospheric superstation and has carried out many atmospheric observations (Ji et al., 2017; Lin et al., 2017; Zhou et al., 2015). TGM was monitored using a TEKRAN 2537X instrument widely used globally for long-term atmospheric Hg observations with high precision and stability. The detailed operational procedures, as well as quality control and quality analysis methods, were detailed in our previous study (Tang et al., 2018). In order to identify the downward trend, we used the seasonal Mann-Kendal (SMK) test for trend analysis and estimation of Sen's slope (Cole et al., 2013; Weiss-Penzias et al., 2016), which is suitable for analyzing environmental data containing a seasonal cycle. The annual slope was the average of the seasonal Sen's slope, as verified by SMK. The specific tasks were conducted using the "mblm" and "Kendall" packages in RStudio 4.0.0.

Surface and upper-air meteorological data were collected from the China Meteorological Data Service Center (http://data.cma.cn/en). The Hybrid Single Particle Lagrangian Integrated Trajectory Model (HYSPLIT, https://www.ready.noaa.gov/HYSPLIT.php) was run for each day to calculate 24 h backward trajectories. Gridded meteorological data at a horizontal resolution of 1 × 1 were obtained from the Global Data Assimilation System (GDAS) (Draxler and Hess, 1998). As no measured planetary boundary layer height data were available, we set the starting height as 500 m above ground level to represent the center height of the boundary layer, where pollutants are usually well-mixed.

Considering the annual or monthly resolution of existing emission inventories (Liu et al., 2018, 2019; Wu et al., 2016), it is difficult to use such results in GAM, where hourly precision is required. Previous studies have generally used CO to represent combustion sources for atmospheric Hg (Jaffe et al., 2005; Zhang et al., 2015a). Given that Hg emissions in Beijing and surrounding provinces are dominated by combustion sources (Liu et al., 2019), we also used CO to represent anthropogenic Hg emissions. CO concentration data were collected from the China National Environmental Monitoring Station (http://beijingair.sinaapp.com, last accessed June 2020).

According to previous studies, GBC accounted for ~60% of the concentration in China (Liu et al., 2019; Wang et al., 2014). As GBC reflects the impact of global emissions, we chose this for the analysis of atmospheric Hg variation in this study. GBC was derived from GEOS-CHEM simulation results, while the simulated spatiotemporal distribution of TGM in China was been obtained in our previous study using GEOS-CHEM (Liu et al., 2019). We excluded anthropogenic emissions in China from the model in order to obtain the GBC value.

2.3. Model validation and result interpretation

2.3.1. Model validation

10-fold cross-validation was carried out to evaluate the accuracy of the GAM model (Figure S3) (Fushiki, 2009). The entire fitting data sets were randomly split into ten subsets, each containing ~10% of the total data. In each round of cross-validation, the nine subsets were used to fit the model and make predictions on the remaining one subset. This process was repeated ten times so that every subset was tested. The agreement between the measured and predicted TGM was evaluated using statistical indicators such as coefficient of determination (R^2).

To examine underlying assumptions regarding homogeneity, normality, and independence of GAM so as to ensure the model's effectiveness and accuracy, we used the following methods: (1) Quantile-quantile (QQ) plots (Sample quantiles against theoretical quantiles, Figure S4a), scatterplots (residuals against linear predictor, Figure S4b), and histograms of the residuals and scatter plots (responses against fitted values) (Figure S4c); (2) Fitted TGM against observed TGM (Fig. 2a) and model residuals (Figure S4d); and (3) Autocorrelation of both the original TGM and residues (Figure S5).

2.3.2. Quantifying the contribution of independent variables

We used a relative importance analysis method to quantify the contribution of each independent variable made toward the dependent variable. This method helps determine the extent to which each variable drives the prediction and allows for more accurate variance partitioning among correlated independent variables (Tonidandel and LeBreton, 2011). It acts as a useful supplement to multiple regression by providing information not readily available from the indices typically produced from a multiple regression analysis. We calculated the relative importance using the "varImp" function in the "caret" package of RStudio 3.6.2 (Kuhn, 2008).

The emission inventory showed the variations in anthropogenic Hg emissions. We first identified the source area by using the Potential Source Contribution Factors (PSCF) method (Polissar et al., 1999). The PSCF value can be used to quantify the impact of source area emissions on the monitored concentration: the higher the value, the larger the contribution of a source area. The PSCF values at a grid cell in the study domain were calculated by counting the endpoints of trajectories terminating within each cell (details given in section S1). We then calculated the emission inventories of the target area using a technology-based emission factor method presented in our previous studies (Liu et al., 2019; Wu et al., 2016; Zhang et al., 2015b). The related parameters were updated based on recent research (Wen et al., 2020). The Hg/CO ratio can also be used to investigate changes in anthropogenic emissions, but has a higher time resolution than the emission inventory method.

3. Results and discussion

3.1. TGM dataset analysis

The annual average TGM concentrations in urban Beijing were 4.61 ng m^{-3} in 2015, declining to 2.72 ng m^{-3} in 2018 at a rate of −0.37 ng m^{-3} yr^{-1} (or −8.0% yr^{-1}, Sen's slope, $p < 0.001$) (Fig. 1). A similarly large TGM reduction (annual decrease rate of 0.60 ng m^{-3} yr^{-1}) was also observed in rural eastern China almost simultaneously (Tang et al., 2018). These observed decreasing trends of atmospheric Hg in China were the most robust among all global Hg observations (Kim et al., 2016; Nguyen et al., 2019; Tang et al., 2018; Zhang et al., 2016). For example,

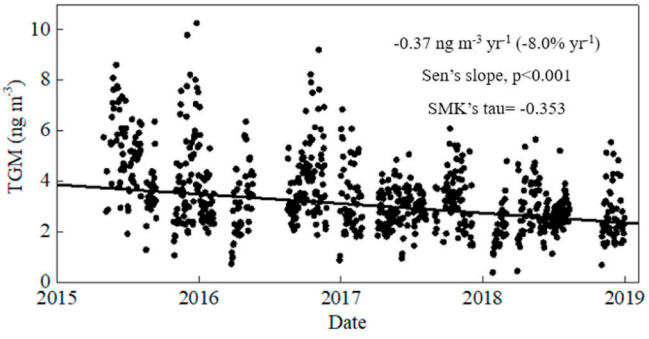

Fig. 1. The times series of TGM concentrations and Sen's slope of daily concentration in Beijing. The black dot was daily average GEM concentration during sampling period.

the 10-year trends of gaseous elemental Hg (GEM) concentrations at six background sites in the Arctic and Canada showed decreasing trends of 13–35 pg m^{-3} yr^{-1} (Cole et al., 2013), while in South Korea, TGM concentrations decreased in urban Seoul after 2011 (Kim et al., 2016).

As for the seasonal downward trend, the decrease in winter (December–February; −0.79 ng m^{-3} yr^{-1}; $p < 0.01$) was significantly higher than for observations in other seasons (−0.39 to −0.50 ng m^{-3} yr^{-1}). These differences in seasonal downward trends imply impacts from time-specific parameters, as explored further in following sections.

3.2. Model validation and interpretation

Fig. 2 compares the observed and fitted TGM; the statistical model explained 56.5% of the variance in Hg concentration and the adjusted R^2 reached 0.547. In other studies using GAM to quantify the impact factors on air pollutant concentrations or variation trends, the adjusted R^2 generally ranged from 0.35 to 0.86 (Aldrin and Haff, 2005; Gong et al., 2018; Li et al., 2019). Thus, the adjusted R^2 for our results was acceptable and the independent variables were deemed capable of interpreting the existing dependent variables. The time series (Fig. 2) showed a generally good agreement between the observed and modeled values and the residuals had an almost normal distribution (Figure S4c). The standard deviation and 95th percentiles of the residuals were 1.05 ng m^{-3} and 5.33 ng m^{-3}, respectively.

The 10-fold cross-validation results showed good coincidence between the GAM and cross-validated results, demonstrating the former's reliability (Figure S3). The QQ plot results showed that GAM produced good results around the average concentration and had elevated uncertainties in larger and smaller values (Figure S4a). The residuals vs. predictors (Figure S4b) and the histogram of residuals (Figure S4c) showed almost unbiased simulations of TGM. The autocorrelations of original TGM and residuals (Figure S5) showed a sharp decrease in autocorrelation results that reflected the lack of a lag day during simulation.

The dominant impact factors included CO, RH_{AVG}, and DOY according to the F test (Table S2). We analyzed the partial responses of the top 3 individual parameters to quantify the influence of each parameter (Fig. 3). CO was the most important parameter for TGM, which increased when CO increased (Fig. 3a), demonstrating that anthropogenic Hg emissions significantly impacted TGM. However, the growth rate (curve slope) of TGM decreased with increasing CO concentrations. In other words, although anthropogenic Hg emissions promoted TGM pollution, the degree of impact decreased with increasing Hg emissions. It is quite possible that increasing Hg emissions also promoted TGM oxidation since the GEM oxidation rate was positively correlated with GEM concentration (Horowitz et al., 2017). Thus, anthropogenic Hg emissions also promoted TGM deposition.

DOY was a comprehensive time-specific meteorological factor that showed lower values in summer and elevated values in winter (Fig. 3b), which we attributed to the impact of atmospheric diffusion conditions such changes in boundary layer height. Such conditions are generally better in summer than in winter (Fu et al., 2015; Mao et al., 2017). The smooth function curve of RH_{AVG} remained relative stable with an overall slight increase when relative humidity (RH) was < ~80%, but increased sharply when RH was > ~80% (Fig. 3c). This indicated that TGM increased with rising RH and that this effect was significant when RH was > ~80%. According to a previous study, particulates in the air convert to an aqueous phase in an elevated RH environment (Horowitz et al., 2017). Under such conditions, the aqueous environment at the particle surface promotes the reduction of oxidized Hg. Thus, particulate-bound Hg (PBM) can be transformed to GEM, while gaseous oxidized Hg (GOM) can dissolve in the water and be reduced to GEM as well. Therefore, the TGM concentration increases due to reduced PBM and decreased overall deposition rate. In addition, high RH provides a stagnant atmospheric environment and hinders the diffusion of pollutants (Horowitz et al., 2017).

3.3. Quantifying the contribution of each independent variable

The contribution of each independent variable was determined by calculating their relative importance (Table 1). CO contributed to 51.5% of total TGM variation, indicating significant impacts from anthropogenic emissions. Differences in meteorological condition contributed to 47.1% of TGM variation. DOY and RH were the two dominant independent meteorological parameters, explaining 11.7% and 10.6% of total variation, respectively. The global background only made up 1.4% of total TGM variation.

3.3.1. Anthropogenic emissions

The relative importance results showed that anthropogenic emissions dominated TGM variation. According to the PSCF results (Figure S5), the dominant source regions of the observed TGM in Beijing included the cities of Beijing and Tianjin along with Hebei Province. To evaluate the GAM results, we calculated the Hg emissions from these regions from 2013 to 2017, during which Hg emissions decreased year by year with a linear fit (Figure S6). We then predicted Hg emissions in 2018 based on the fitting function, finding that these decreased from 47 t in 2015 to 35 t in 2018, down ~26%. According to Section 3.1, annual TGM decreased by 41% between 2015 and 2018, such that the decrease in Hg emissions could explain almost 63% of the TGM decrease based on crude estimation, quite similar to GAM result. The reduction in anthropogenic emissions driving the downward TGM trend was also verified by previous observation and modeling studies (Liu et al., 2019; Zhang et al., 2019).

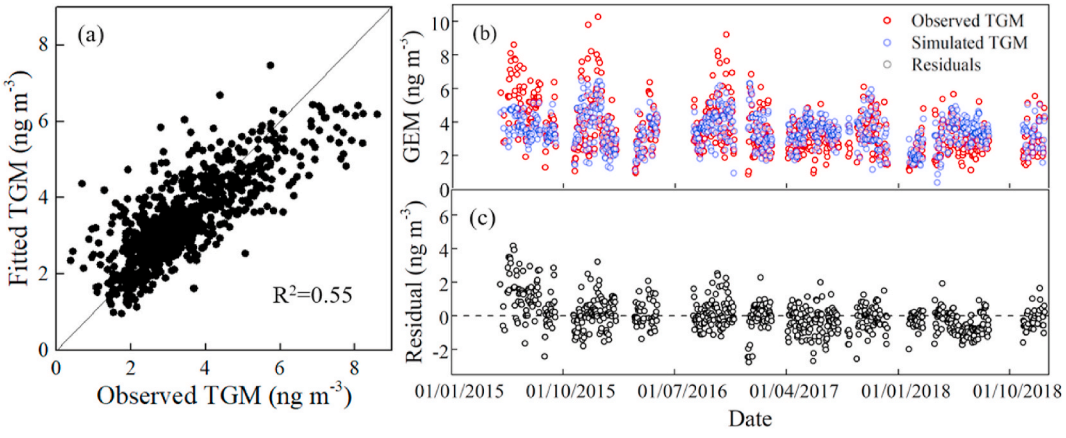

Fig. 2. GAM results (a) the fitted TGM vs observed TGM (b) the time series of observed TGM, simulated TGM and residuals.

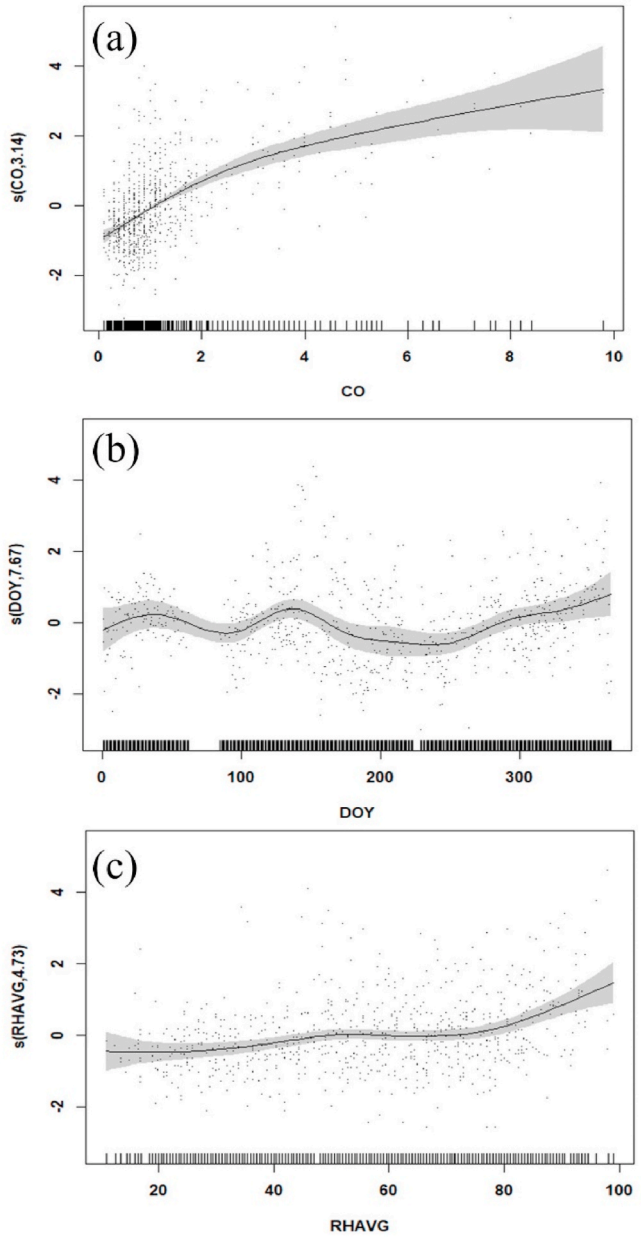

Fig. 3. Spline of TGM to individual parameters (a) CO, (b) DOY, (c) RHAVG. The grey background around the line are 95% confidence bounds for the response. The short lines on x axes show the distribution of data points. The number in the bracket of ordinate title is the estimated degree of freedom. The dots in the figure are the residuals.

The TGM decline peaked in winter while the decrease in autumn was minimal (Figure S6). According to the emission inventory, the emission decline in winter reached 32%, much higher than the results in other seasons (26–27%) (Table S3). This especially obvious decline in winter was due to the substitution of coal with natural gas or electricity during heating season (Nov 15 through March 15) and off-peak industrial production during winter (Fig. 4). These actions reduced the consumption of coal and other raw materials where Hg was an impurity, which further led to the decrease of atmospheric Hg emissions in source areas and TGM concentrations in Beijing. The seasonal decline in Hg emissions could be validated by the Hg/CO ratios for power plants (25.2), industrial boilers (2.9), and residential coal combustion (0.4) (Wang et al., 2005; Wu et al., 2006). We observed a decreasing Hg/CO ratio throughout the spring, summer, and autumn (Figure S8), which we

Table 1
Relative importance of independent variables.

Variable name	Description	Identification	Relative importance
CO	Average CO concentration	Anthropogenic emission	51.5%
RH_{AVG}	Average relative humidity	Surface air meteorological condition	10.6%
P	Average pressure	Surface air meteorological condition	5.8%
V_{AVG}	Average wind speed	Surface air meteorological condition	4.7%
T_{DELTA}	Temperature difference	Surface air meteorological condition	4.5%
DOY	Day of the year	Synthetical meteorological condition	11.7%
Temp700	Temperature at 700 mb	Regional transportation	7.3%
$Traj_{Long}$	Longitude after 24 h backward trajectory	Regional transportation	2.5%
GBC	Global background concentration	Global background concentration	1.4%

attributed to emission reductions from sources with high Hg/CO, such as power plants. The ultra-low emission standard in coal-fired power plants led to significant Hg emission reductions from 2013 to 2017 (Fig. 4). In winter, the substitution of coal with natural gas or electricity in rural northern China during winter led to dramatic decreases in emissions from residential coal combustion (Fig. 4); the low Hg/CO ratio of this source means that such reductions would increase Hg/CO in the ambient air. This mutual authentication between the Hg emission inventory and Hg/CO ratio verified the feasibility of characterizing atmospheric Hg emissions using CO as applied in this study.

3.3.2. Meteorological conditions

Meteorological conditions influence the reemission, transport, and diffusion of atmospheric Hg; these contributed to decreasing TGM concentration in Beijing at a level nearly equal to anthropogenic Hg emissions. An analysis of $PM_{2.5}$ pollution from 2015 to 2018 also found that the meteorology with better diffusion condition improved air quality, indicating the overall positive effect of meteorological conditions on the mitigation of air pollution in Beijing (Li et al., 2019).

Surface meteorological conditions important for TGM variation in this study included RH, P, V_{AVG}, and T_{DELTA}. These affected TGM by Hg dilution, evaporation, and transformation, contributing to 25.6% of TGM variation. RH was the most dominant of all surface meteorological parameters considered for reasons explained in Section 3.2. The frequency of high-RH events (RH > 80%) in 2015 reached 26.5% of total sampling days (Table 2), but fell to ~10.2–12.5% in the other years. This clear reduction in frequency of high-RH events from 2015 to 2018 made RH an important independent variable influencing TGM variation during the study period. Enhanced V_{AVG} and low P also accelerated the evaporation and dilution of TGM, jointly leading to 10.5% of atmospheric Hg decrease. The average wind velocity in 2015 was ~2.64 ± 1.30 $m^3\ s^{-1}$, much lower than that in other years. The atmospheric pressure in 2015 was 10154 ± 108 Pa, lower than in 2017 and 2018 (Table 2). T_{DELTA} variation accounted for 4.5% of variation from 2015 to 2018. Sunny and rainy days provide good diffusion and convection conditions, respectively, which would be reflected in T_{DELTA} and lead to lower TGM.

DOY contributed to 11.7% of total TGM variation, acting as a complementary synthetic meteorological condition that reflects diffusion processes such as boundary layers and convection conditions that are not characterized by current meteorological data. The contribution of

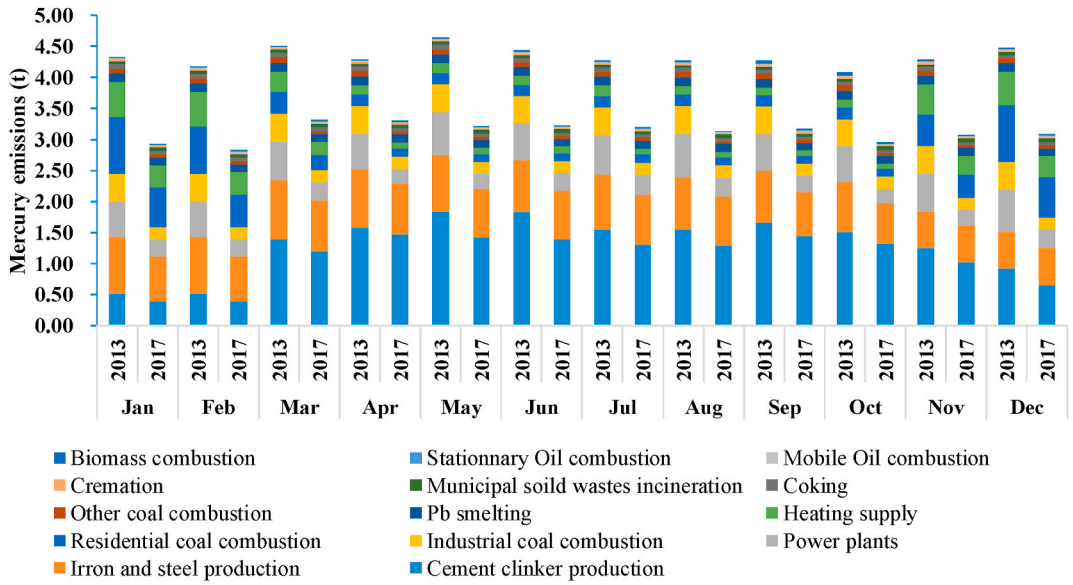

Fig. 4. Monthly Hg emissions by sector in 2013 and 2017.

Table 2
The annual variation of dominant meteorological parameters.

Variables	Studied year			
	2015	2016	2017	2018
Frequency of high RH (RH_{AVG}>80%)	26.7%	12.8%	10.5%	10.2%
P (Pa)	10154 ± 108	10189 ± 98	10163 ± 106	10145 ± 110
V_{AVG} (m s^{-1})	2.64 ± 1.30	2.95 ± 1.41	2.92 ± 1.44	2.74 ± 1.21
T_{DELTA} (°C)	10.14 ± 4.09	11.69 ± 3.78	12.53 ± 4.58	11.40 ± 4.96
$Temp_{700}$ (°C)	−0.58 ± 8.24	−3.47 ± 9.21	−1.85 ± 9.19	−1.66 ± 11.19

DOY in this study indicated a significant impact of diffusion conditions on TGM concentrations. The boundary layer height was lower in winter while convection always existed in summer (Figure S7), indicating that the reduced diffusion and convection conditions in winter were detrimental to the mitigation of TGM pollution.

Regional transportation also affected TGM variation by 9.8% during the sampling period. Compared to the non-significant effect of $Traj_{La}$, $Traj_{Long}$ contributed to 2.5% of total TGM decrease, indicating that longitudinal transportation of TGM was much more important than latitudinal transportation to TGM concentration in Beijing. According to Hua et al. (2018), the transmission channels of atmospheric pollutants affecting Beijing mainly pass through cities in the provinces of Shandong, Shanxi, and Henan, generally located south of Beijing. From 2015 to 2018, stricter control measures for air pollutants also led to significant Hg emission reductions in these areas and reduced the impact of long-range transportation on Beijing (Liu et al., 2019). $Temp_{700}$ accounted for 7.3% of TGM variation from 2015 to 2018, reflecting large-scale vertical airmass circulation and airmass exchange. Higher $Temp_{700}$ in 2015 implied a smaller temperature gradient between the middle atmosphere and the surface, driving the vertical diffusion of TGM.

3.3.3. Global background concentration

GBC is an important part of local TGM concentrations (Pirrone et al., 2010). In the northern hemisphere, TGM measurements at background sites ranged from 1.3 to 1.5 ng m^{-3} (Sprovieri et al., 2017), accounting for ~28–55% of annual TGM monitored in Beijing. However, GBC only contributed to 1.4% of the total TGN variation in Beijing in our study, indicating that although GBC accounts for a large proportion of atmospheric Hg, variations in GBC were less important in driving the observed decrease in TGM in Beijing. However, this does not mean that GBC variations should be excluded from the independent parameters in GAM, because global Hg reductions will increase the contribution of GBC at remote and suburban sites.

3.4. Conclusions

We used GAM to explain variations in observed Hg concentration trends in Beijing, China by coupling the model with parameters representing GBC, anthropogenic emissions, and meteorological conditions; reductions in these explained 1.4%, 51.5%, and 47.1% of the decrease in airborne Hg concentration, respectively. Compared to chemical transport models, GAM assessment requires easily obtained meteorological parameters and uses a relatively simple computation process, making it suitable for rapid assessments. After the implementation of the *Minamata Convention on Mercury*, signatories face pressure to reduce Hg emissions and take corresponding actions. GAM provides a rapid and effective alternative for exploring long-term changes in atmospheric Hg and influential factors at the city level.

We used the "identity link" function with Gaussian distribution because we assumed a normal distribution of TGM concentrations, but the TGM concentrations actually had a lognormal distribution (Figure S1). For improved normality within GAM, it would be better to conduct logarithmic transformations of TGM, in which results' relative importance reflects the contributions of each independent variable to changes in the log concentration of TGM. Thus, it was difficult to calculate the direct contribution to TGM variation. The statistical model represented 56.7% of the variance in Hg concentration and the adjusted R^2 reached 0.551 after log transformation of TGM, almost the same as when using normal assumptions. In addition, the approximate significance of the smoothed terms were almost the same, according to Table S2. Thus, the normality assumption for TGM would not change our basic conclusions.

In future, when applying GAM at other sites, the distribution characteristics of target air pollutants should be analyzed before determining the characteristics of link functions and the representativeness of CO for anthropogenic emissions should be considered. At our study sites, combustion sources were the dominant sources and we demonstrated the feasibility of this assumption. However, for sites impacted by non-

combustion sources such as primary Hg production or artisanal gold production, such assumptions would be less reliable. To extend the applicability of this model, we recommend developing GAM with the Hidden Markov Model to avoid unavailable parameters.

CRediT authorship contribution statement

Qingru Wu: Writing - original draft, designed the research, wrote the manuscript, with contributions from all other co-authors, have equal contribution. **Yi Tang:** Writing - original draft, designed the research, wrote the manuscript with contributions from all other co-authors, have equal contribution. **Shuxiao Wang:** Writing - original draft, designed the research, wrote the manuscript with contributions from all other co-authors. **Liang Li:** performed the research. **Guigang Tang:** Research administration, performed the research. **Kaiyun Liu:** Writing - original draft, wrote the manuscript with contributions from all other co-authors.

Declaration of competing interest

The authors declare that they have no known competing financial interests or personal relationships that could have appeared to influence the work reported in this paper.

Acknowledgements

This work is sponsored by the Natural Science Foundation of China (No. 21607090& 21625701) and National Key Research and Development Program of China (No. 2016YFC0201800). We thank Shanghai Huachuan Environment Technology Corp for the instrument maintenance and quality control.

Appendix A. Supplementary data

Supplementary data related to this article can be found at https://doi.org/10.1016/j.atmosenv.2020.117868.

References

Aldrin, M., Haff, I., 2005. Generalised additive modelling of air pollution, traffic volume and meteorology. Atmos. Environ. 39, 2145–2155.
Cole, A.S., Steffen, A., Pfaffhuber, K.A., Berg, T., Pilote, M., Poissant, L., Tordon, R., Hung, H., 2013. Ten-year trends of atmospheric mercury in the high Arctic compared to Canadian sub-Arctic and mid-latitude sites. Atmos. Chem. Phys. 13, 1535–1545.
Davis, J.M., Speckman, P., 1999. A model for predicting maximum and 8h average ozone in Houston. Atmos. Environ. 33, 2487–2500.
Draxler, R.R., Hess, G.D., 1998. An overview of the hysplit-4 modeling system for trajectories. Aust. Meteorol. Mag. 47, 295–308.
Fu, X.W., Zhang, H., Yu, B., Wang, X., Lin, C.J., Feng, X.B., 2015. Observations of atmospheric mercury in China: a critical review. Atmos. Chem. Phys. 15, 9455–9476.
Fushiki, T., 2009. Estimation of prediction error by using K-fold cross-validation. Stat. Comput. 21, 137–146.
Gong, X., Hong, S., Jaffe, D.A., 2018. Ozone in China: spatial distribution and leading meteorological factors controlling O3 in 16 Chinese cities. Aerosol and Air Quality Research 18, 2287–2300.
Gong, X., Kaulfus, A., Nair, U., Jaffe, D.A., 2017. Quantifying O3 impacts in urban areas due to wildfires using a generalized additive model. Environ. Sci. Technol. 51, 13216–13223.
Holland, D.M., Principe, P.P., Sickles, J.E., 2000. Trends in atmospheric sulfur and nitrogen species in the eastern United States for 1989-1995. Atmos. Environ. 33, 37–49.
Horowitz, H.M., Jacob, D.J., Zhang, Y., Dibble, T.S., Slemr, F., Amos, H.M., Schmidt, J. A., Corbitt, E.S., Marais, E.A., Sunderland, E.M., 2017. A new mechanism for atmospheric mercury redox chemistry: implications for the global mercury budget. Atmos. Chem. Phys. Discuss. 1–33.
Hua, Y., Wang, S.X., Jiang, J.K., Zhou, W., Xu, Q.C., Li, X.X., Liu, B.X., Zhang, D.W., Zheng, M., 2018. Characteristics and sources of aerosol pollution at a polluted rural site southwest in Beijing, China. Sci. Total Environ. 626, 519–527.
Jaffe, D., Prestbo, E., Swartzendruber, P., Weisspenzias, P., Kato, S., Takami, A., Hatakeyama, S., Kajii, Y., 2005. Export of atmospheric mercury from Asia. Atmos. Environ. 39, 3029–3038.
Ji, D., Li, L., Pang, B., Xue, P., Wang, L., Wu, Y., Zhang, H., Wang, Y., 2017. Characterization of black carbon in an urban-rural fringe area of Beijing. Environ. Pollut. 223, 524–534.
Kim, K.-H., Brown, R.J.C., Kwon, E., Kim, I.-S., Sohn, J.-R., 2016. Atmospheric mercury at an urban station in Korea across three decades. Atmos. Environ. 131, 124–132.
Kuhn, M., 2008. Building predictive models in R using the caret package. J. Stat. Software 28, 1–26.
Li, K., Jacob, D.J., Liao, H., Shen, L., Zhang, Q., Bates, K.H., 2019. Anthropogenic drivers of 2013-2017 trends in summer surface ozone in China. Proc. Natl. Acad. Sci. U. S. A. 116, 422–427.
Lin, H., Liu, T., Fang, F., Xiao, J., Zeng, W., Li, X., Guo, L., Tian, L., Schootman, M., Stamatakis, K.A., Qian, Z., Ma, W., 2017. Mortality benefits of vigorous air quality improvement interventions during the periods of APEC Blue and Parade Blue in Beijing, China. Environ. Pollut. 220, 222–227.
Liu, K.Y., Wang, S.X., Wu, Q.R., Wang, L., Ma, Q., Zhang, L., Li, G.L., Tian, H.Z., Duan, L., Hao, J.M., 2018. A highly resolved mercury emission inventory of Chinese coal-fired power plants. Environ. Sci. Technol. 52, 2400–2408.
Liu, K.Y., Wu, Q.R., Wang, L., Wang, S.X., Liu, T.H., Ding, D., Tang, Y., Li, G.L., Tian, H. Z., Duan, L., Hao, J.M., 2019. Substantial reduction in atmospheric mercury concentration as a co benefit of China's clean air action plan during 2013-2017. Environ. Sci. Technol.
Mao, H., Hall, D., Ye, Z., Zhou, Y., Felton, D., Zhang, L., 2017. Impacts of large-scale circulation on urban ambient concentrations of gaseous elemental mercury in New York, USA. Atmos. Chem. Phys. 17, 11655–11671.
Nguyen, L.S.P., Sheu, G.R., Lin, D.W., Lin, N.H., 2019. Temporal changes in atmospheric mercury concentrations at a background mountain site downwind of the East Asia continent in 2006-2016. Sci. Total Environ. 686, 1049–1056.
Pacyna, J.M., Travnikov, O., De Simone, F., Hedgecock, I.M., Sundseth, K., Pacyna, E.G., Steenhuisen, F., Pirrone, N., Munthe, J., Kindbom, K., 2016. Current and future levels of mercury atmospheric pollution on a global scale. Atmos. Chem. Phys. 16, 12495–12511.
Pirrone, N., Cinnirella, S., Feng, X., Finkelman, R.B., Friedli, H.R., Leaner, J., Mason, R., Mukherjee, A.B., Stracher, G.B., Streets, D.G., Telmer, K., 2010. Global mercury emissions to the atmosphere from anthropogenic and natural sources. Atmos. Chem. Phys. 10, 5951–5964.
Polissar, A.V., Hopke, P.K., Paatero, P., Kaufmann, Y.J., Hall, D.K., Bodhaine, B.A., Dutton, E.G., Harris, J.M., 1999. The aerosol at Barrow, Alaska: long-term trends and source locations. Atmos. Environ. 33, 2441–2458.
Reiss, R., 2006. Temporal trends and weekend–weekday differences for benzene and 1,3-butadiene in Houston, Texas. Atmos. Environ. 40, 4711–4724.
Saiz-Lopez, A., Sitkiewicz, S.P., Roca-Sanjuan, D., Oliva-Enrich, J.M., Davalos, J.Z., Notario, R., Jiskra, M., Xu, Y., Wang, F., Thackray, C.P., Sunderland, E.M., Jacob, D. J., Travnikov, O., Cuevas, C.A., Acuna, A.U., Rivero, D., Plane, J.M.C., Kinnison, D. E., Sonke, J.E., 2018. Photoreduction of gaseous oxidized mercury changes global atmospheric mercury speciation, transport and deposition. Nat. Commun. 9, 4796.
Selin, N.E., Jacob, D.J., Yantosca, R.M., Strode, S., Jaeglé, L., Sunderland, E.M., 2008. Global 3-D land-ocean-atmosphere model for mercury: present-day versus preindustrial cycles and anthropogenic enrichment factors for deposition. Global Biogeochem. Cycles 22, 379–389.
Sprovieri, F., Pirrone, N., Bencardino, M., Amp, Apos, Amore, F., Angot, H., Barbante, C., Brunke, E.-G., Arcega-Cabrera, F., Cairns, W., Comero, S., Diéguez, M.d.C., Dommergue, A., Ebinghaus, R., Feng, X.B., Fu, X., Garcia, P.E., Gawlik, B.M., Hageström, U., Hansson, K., Horvat, M., Kotnik, J., Labuschagne, C., Magand, O., Martin, L., Mashyanov, N., Mkololo, T., Munthe, J., Obolkin, V., Ramirez Islas, M., Sena, F., Somerset, V., Spandow, P., Vardè, M., Walters, C., Wängberg, I., Weigelt, A., Yang, X., Zhang, H., 2017. Five-year records of mercury wet deposition flux at GMOS sites in the Northern and Southern hemispheres. Atmos. Chem. Phys. 17, 2689–2708.
Tai, A.P.K., Mickley, L.J., Jacob, D.J., 2010. Correlations between fine particulate matter (PM2.5) and meteorological variables in the United States: implications for the sensitivity of PM2.5 to climate change. Atmos. Environ. 44, 3976–3984.
Tang, Y., Wang, S., Wu, Q., Liu, K., Wang, L., Li, S., Gao, W., Zhang, L., Zheng, H., Li, Z., Hao, J., 2018. Recent decrease trend of atmospheric mercury concentrations in East China: the influence of anthropogenic emissions. Atmos. Chem. Phys. 18, 8279–8291.
Tong, Y., Yin, X., Lin, H., Buduo, Danzeng, Wang, H., Deng, C., Chen, L., Li, J., Zhang, W., Schauer, J.J., Kang, S., Zhang, G., Bu, X., Wang, X., Zhang, Q., 2016. Recent decline of atmospheric mercury recorded by androsace tapete on the Tibetan plateau. Environ. Sci. Technol. 50, 13224–13231.
Tonidandel, S., LeBreton, J.M., 2011. Relative importance analysis: a useful supplement to regression analysis. J. Bus. Psychol. 26, 1–9.
UNEP, 2013. Minamata Convention on Mercury. UNEP, Minamata, Japan.
Wang, L., Wang, S., Zhang, L., Wang, Y., Zhang, Y., Nielsen, C., McElroy, M.B., Hao, J., 2014. Source apportionment of atmospheric mercury pollution in China using the GEOS-Chem model. Environ. Pollut. 190, 166–175.
Wang, L.T., Zhang, Q., Hao, J.M., He, K.B., 2005. Anthropogenic CO emission inventory of Mainland China. Acta Sci. Circumstantiae 25, 1580–1585.
Weigelt, A., Ebinghaus, R., Manning, A.J., Derwent, R.G., Simmonds, P.G., Spain, T.G., Jennings, S.G., Slemr, F., 2015. Analysis and interpretation of 18 years of mercury observations since 1996 at Mace Head, Ireland. Atmos. Environ. 100, 85–93.
Weiss-Penzias, P.S., Gay, D.A., Brigham, M.E., Parsons, M.T., Gustin, M.S., Ter Schure, A., 2016. Trends in mercury wet deposition and mercury air concentrations across the U.S. and Canada. Sci. Total Environ. 568, 546–556.
Wen, M., Wu, Q., Li, G., Wang, S., Li, Z., Tang, Y., et al., 2020. Impact of ultra-low emission technology retrofit on the mercury emissions and cross-media transfer in coal-fired power plants. J. Hazard Mater. 396, 122729.

Wood, S.N., 2017. Generalized Additive Models: an Introduction with R, second ed. CRC Press.
Wu, Q., Li, G., Wang, S., Liu, K., Hao, J., 2018a. Mitigation options of atmospheric Hg emissions in China. Environ. Sci. Technol.
Wu, Q., Wang, S., Liu, K., Li, G., Hao, J., 2018b. Emission-limit-oriented strategy to control atmospheric mercury emissions in coal-fired power plants toward the implementation of the Minamata convention. Environ. Sci. Technol. 52, 11087–11093.
Wu, Q.R., Wang, S.X., Li, G.L., Liang, S., Lin, C.J., Wang, Y., Cai, S.Y., Liu, K.Y., Hao, J. M., 2016. Temporal trend and spatial distribution of speciated atmospheric mercury emissions in China during 1978-2014. Environ. Sci. Technol. 50, 13428–13435.
Wu, Y., Wang, S.X., Streets, D.G., Hao, J.M., Chan, M., Jiang, J.K., 2006. Trends in Anthropogenic Mercury Emissions in china from 1995 to 2003. Environmental Science & Technology.
Ye, Z., Mao, H., Driscoll, C.T., Wang, Y., Zhang, Y., Jaeglé, L., 2018. Evaluation of CMAQ coupled with a state-of-the-art mercury chemical mechanism (CMAQ-newHg-Br). J. Adv. Model. Earth Syst. 10, 668–690.
Zhang, H., Fu, X.W., Lin, C.J., Wang, X., Feng, X.B., 2015a. Observation and analysis of speciated atmospheric mercury in Shangri-La, Tibetan Plateau, China. Atmos. Chem. Phys. 15, 653–665.
Zhang, L., Wang, S.X., Wang, L., Wu, Y., Duan, L., Wu, Q.R., Wang, F.Y., Yang, M., Yang, H., Hao, J.M., Liu, X., 2015b. Updated emission inventories for speciated atmospheric mercury from anthropogenic sources in China. Environ. Sci. Technol. 49, 3185–3194.
Zhang, Q., Zheng, Y., Tong, D., Shao, M., Wang, S., Zhang, Y., Xu, X., Wang, J., He, H., Liu, W., Ding, Y., Lei, Y., Li, J., Wang, Z., Zhang, X., Wang, Y., Cheng, J., Liu, Y., Shi, Q., Yan, L., Geng, G., Hong, C., Li, M., Liu, F., Zheng, B., Cao, J., Ding, A., Gao, J., Fu, Q., Huo, J., Liu, B., Liu, Z., Yang, F., He, K., Hao, J., 2019. Drivers of Improved PM2.5 Air Quality in China from 2013 to 2017. Proc Natl Acad Sci U S A.
Zhang, Y., Jacob, D.J., Horowitz, H.M., Chen, L., Amos, H.M., Krabbenhoft, D.P., Slemr, F., St Louis, V.L., Sunderland, E.M., 2016. Observed decrease in atmospheric mercury explained by global decline in anthropogenic emissions. Proc. Natl. Acad. Sci. U.S.A. 113, 526.
Zhou, Y., Cheng, S., Chen, D., Lang, J., Wang, G., Xu, T., Wang, X., Yao, S., 2015. Temporal and spatial characteristics of ambient air quality in beijing, China. Aerosol Air Qual. Res. 15, 1868–1880.